Earth Syst. Dynam. Discuss., 6, 1395–1443, 2015
www.earth-syst-dynam-discuss.net/6/1395/2015/
doi:10.5194/esdd-6-1395-2015

Earth System Dynamics
Discussions
Open Access

An ice sheet model of reduced complexity for paleoclimate studies

B. Neff[1,2], A. Born[1,2], and T. F. Stocker[1,2]

[1]Climate and Environmental Physics, Physics Institute, University of Bern, Bern, Switzerland
[2]Oeschger Centre for Climate Change Research, Bern, Switzerland

Received: 9 July 2015 – Accepted: 19 July 2015 – Published: 11 August 2015

Correspondence to: A. Born (born@climate.unibe.ch)

Published by Copernicus Publications on behalf of the European Geosciences Union.

An ice sheet model of reduced complexity for paleoclimate studies
B. Neff et al.

Abstract

IceBern2D is a vertically integrated ice sheet model to investigate the ice distribution on long timescales under different climatic conditions. It is forced by simulated fields of surface temperature and precipitation of the last glacial maximum and present day climate from a comprehensive climate model. This constant forcing is adjusted to changes in ice elevation. Bedrock sinking and sea level are a function of ice volume. Due to its reduced complexity and computational efficiency, the model is well-suited for extensive sensitivity studies and ensemble simulations on extensive temporal and spatial scales. It shows good quantitative agreement with standardized benchmarks on an artificial domain (EISMINT). Present day and last glacial maximum ice distributions on the Northern Hemisphere are also simulated with good agreement. Glacial ice volume in Eurasia is underestimated due to the lack of ice shelves in our model.

The efficiency of the model is utilized by running an ensemble of 400 simulations with perturbed model parameters and two different estimates of the climate at the last glacial maximum. The sensitivity to the imposed climate boundary conditions and the positive degree day factor β, i.e., the surface mass balance, outweighs the influence of parameters that disturb the flow of ice. This justifies the use of simplified dynamics as a means to achieve computational efficiency for simulations that cover several glacial cycles. The sensitivity of the model to changes in surface temperature is illustrated as a hysteresis based on 5 million year long simulations.

1 Introduction

The understanding of the Earth's climate on time scales longer than about 100 000 years (100 kyr) critically depends on the build-up and demise of continental ice sheets. Over the past several million years, its number alternated between the two that are present today on Greenland and Antarctica and four, with two additional masses of ice over both North America and Eurasia. Among other consequences, this caused sea

ESDD
6, 1395–1443, 2015

level to drop in excess of 120 m during the most recent glaciation (Waelbroeck et al., 2002), exposing currently submerged land that allowed humans to first arrive and settle on the American (Dixon, 2001) and Australian continents (Forster, 2004).

Proxy records from deep sea sediments show that ice volume varied predominantly on time scales of 41 kyr between 3 and 0.8 million years ago, and with a 100 kyr periodicity more recently (Lisiecki and Raymo, 2005). This is somewhat inconsistent with the prevailing theory that ice sheet volume is dominated by the intensity of Northern Hemisphere summer insolation causing ice to melt (Milankovitch, 1941), because summer insolation on the Northern Hemisphere varies predominantly on the precessional time scale of 23 kyr (Berger, 1978).

Several ice sheet-climate interactions have been proposed to explain this nonlinear response of ice volume to the orbital forcing. Besides the closure of ocean pathways mentioned above, the rerouting of freshwater by ice sheets also has a profound impact on the ocean circulation and sea ice distribution (Stocker, 2013), potentially changing moisture availability for ice sheet growth (Gildor and Tziperman, 2001). Similarly, meridional water transport from the tropics to high latitudes, arguably controlled by insolation gradients instead of absolute values, has been suggested as a limiting factor of ice sheet growth (Raymo and Nisancioglu, 2003). Topographic changes due to the accumulation of ice changes the atmospheric circulation on local (Merz et al., 2014a, b) and hemispheric scales (Li and Battisti, 2008; Pausata et al., 2011; Merz et al., 2013). As ice sheets are usually brighter than the surface they replace, they impact the planetary radiation balance in the short wavelength part of the spectrum (Cess et al., 1991). The long wavelength radiation balance also changes with the growth of ice sheets as the concentration of atmospheric greenhouse gases closely follows global ice sheet volume (Loulergue et al., 2008; Lüthi et al., 2008; Schilt et al., 2010). Probable causes include changes in the ocean circulation (Archer et al., 2000; Fischer et al., 2010) and terrestrial peatlands (Xu-Ri and Prentice, 2008; Spahni et al., 2013). Lastly, ice sheets interact with the lithosphere, sinking into their beds when growing and thereby shifting their surface mass balance toward negative values (Oerlemans, 1981b).

ESDD
6, 1395–1443, 2015

Although these basic components are easily understood at their individual level, the full picture is very complex so that comprehensive numerical modeling is necessary to quantify the underlying physical processes. The often prohibitive cost to run climate models over periods of several millennia has limited such attempts to either using somewhat arbitrary methods to reduce simulation time (e.g., Herrington and Poulsen, 2011; Abe-Ouchi et al., 2013; Heinemann et al., 2014) or the use of climate models of reduced complexity (e.g., Gallée et al., 1992; Smith et al., 2003; Charbit et al., 2007; Bonelli et al., 2009; Robinson et al., 2011). However, in spite of their focus on numerical efficiency, the ice sheet models used in some of the latter studies rival their climate model counterparts in complexity and computational cost, which is not justified for all applications. Importantly, the use of complex ice sheet and ice shelf dynamics consumes resources that in specific cases would better be used for advanced surface mass balance schemes or a probabilistic analysis of many repeated simulations.

In this study, we present a vertically integrated ice sheet model (IceBern2D) that is efficient enough to add only a small computational overhead even to the fastest coarse resolution climate models. This enables simulations spanning several glacial cycles. Similar models that have successfully been employed in the past on a hemispheric scale (Neeman et al., 1988; Verbitsky and Oglesby, 1992) and for regional applications (Oerlemans, 1981a; Siegert and Marsiat, 2001; Plummer and Phillips, 2003; Näslund et al., 2003). The dynamics are similar to early one-dimensional models (Oerlemans, 1981b, 1982), but calculated on a two-dimensional grid. This type of model has been found to produce results similar to three-dimensional thermomechanical models (Calov and Marsiat, 1998).

The IceBern2D model is described in detail in Sect. 2. It is found to perform well in idealized experiments (EISMINT, Huybrechts et al., 1996, Sect. 3) as well as in simulations under continuous Last Glacial Maximum (LGM) and preindustrial climate forcing (Sect. 4.2). We take advantage of the efficiency of the model by using a large ensemble of simulations to estimate the best combination of model parameters (Sect. 4.1). The multi-stability of the Northern Hemisphere ice sheets is investigated in idealized

ESDD
6, 1395–1443, 2015

experiments of five million years duration (Sect. 4.3). We summarize and discuss these results in Sect. 5 and provide an outlook on future directions in Sect. 6.

2 Model formulation

The IceBern2D model is designed to investigate the two dimensional flow of ice and its distribution under different climatic conditions. Therefore, the physical basis of the model is focused on the most important processes. It is based on the conservation of mass and simulates the ice flow in two dimensions, the vertical flow of ice is not simulated explicitly. The forcing of the model is deliberately chosen to only include precipitation and temperature in order to allow for a wide range of usage scenarios with coupled and uncoupled climate models, observational data and possibly climate proxy reconstructions.

The model is based on different physical and empirical constants. Empirical constants are primarily determined from present-day conditions and may vary under different climates and geographical locations. Therefore, these values are used as tuning parameters for different simulations in a common ensemble and marked in Table 1.

The IceBern2D model is discretized on a C-grid (Arakawa and Lamb, 1977). The staggered C-grid is characterized by a combination of calculated values at the center and the border of the grid. This combination yields the most stable results in our simulations.

2.1 Ice dynamics

The basis of the model is formed by the conservation of ice volume in time (Oerlemans, 1981b; Huybrechts et al., 1996). The rate of change of ice thickness h with time is formulated as

$$\frac{\partial h}{\partial t} = \nabla \cdot D \nabla Z + \mathrm{SMB}, \tag{1}$$

Discussion Paper | Discussion Paper | Discussion Paper | Discussion Paper |
ESDD
6, 1395–1443, 2015
An ice sheet model of reduced complexity for paleoclimate studies
B. Neff et al.

where SMB represents the annual net surface mass balance which is described in Sect. 2.2. The flow of ice takes the form of a diffusion with the nonlinear diffusivity D detailed below and the gradient of the ice surface elevation Z a.s.l.. Z is the sum of bedrock elevation B and ice thickness h. The vector differential operator (∇) is defined for the two lateral dimensions.

The diffusivity D is calculated from Glen's flow law (Glen, 1955) by assuming that longitudinal stresses can safely be neglected over the much higher shearing of horizontal planes. This is the so-called "shallow ice approximation" (Hutter, 1983) that can be justified by the fact that the grid spacing is at least a factor of ten greater than the vertical extension of the ice. To obtain the ice volume flow, the flow law is integrated over the full height (Huybrechts et al., 1996) so that:

$$D = \frac{2EA(\rho g)^n}{n+2} h^{n+2} \left[\left(\frac{\partial Z}{\partial x} \right)^2 + \left(\frac{\partial Z}{\partial y} \right)^2 \right]^{\frac{(n-1)}{2}}, \tag{2}$$

where A and n are two empirical parameters determined from a power-law fit of strain rate and effective shear stress. A generally depends on the temperature of the ice which can not be calculated here due to the missing vertical coordinate. We therefore chose a constant value. The plasticity and hence its flow velocity can be modified by an empirical enhancement parameter E which is commonly used to parameterize the softer, impurity-rich glacial ice (Fisher and Koerner, 1986). ρ and g are the density of ice and the gravitational acceleration, respectively (Table 1).

Bedrock relaxation

Thick ice sheets exert a substantial mass load on the underlying bedrock. This leads in equilibrium to an isostatic sinking of the bedrock by about one third, corresponding to the inverse ratio of rock and ice density $\frac{\rho_{\text{rock}}}{\rho_{\text{ice}}} \approx 3$, the hydrostatic equilibrium. This is an important mechanism because it influences the melting of the ice. When the bedrock yields under the pressure of the ice, the top of the ice sheet sinks to a lower and warmer

ESDD
6, 1395–1443, 2015

position. The temperature difference promotes melting and thereby feeds back to the surface mass balance.

A simple yet effective formulation of the bedrock adjustment is the exponential sinking toward its hydrostatic equilibrium (Oerlemans, 1981b):

$$\frac{\partial B}{\partial t} = -\tau_{\mathrm{br}}^{-1}\left(\frac{\rho_{\mathrm{rock}}}{\rho_{\mathrm{ice}}}h + B - B_0\right). \tag{3}$$

B is the bedrock elevation, B_0 is the elevation of the bedrock without ice load and h represents the ice thickness. The relaxation time τ_{br} represents a characteristic time it takes to restore equilibrium. A common value for τ_{br} for is 3000 years (Huybrechts, 2002), but the value may vary locally. Therefore τ_{br} is used as a tuning parameter here (Table 3). Equation (3) is a simplified representation of mass flow in the Earth's upper mantle. It only affects the local grid point and no surrounding fields which is considered sufficient for the purpose of an ice sheet model of reduced complexity.

For the elevation of the bedrock without ice load (B_0) ETOPO1 (Amante and Eakins, 2009) is used. ETOPO1 has a resolution of one arc-minute and distinguishes between bedrock and ice surface. For our application the resolution is linearly interpolated to a stereographic grid of 40 km resolution. It is assumed that ice and bedrock in Greenland are close to isostatic equilibrium today. Thus, B_0 is estimated by adding one third of the ice thickness to the bedrock elevation which corresponds to the mentioned inverse ratio of rock and ice density. In the model domain and at 40 km resolution, this adjustment of the bedrock only affects Greenland.

2.2 Surface mass balance

The surface mass balance (SMB), the difference of the accumulation and ablation, determines where the ice sheet gains or loses mass and thereby drives the flow of the ice sheet. SMB is calculated from daily surface air temperature and precipitation fields. These data are obtained from simulations using the Community Climate System Model version 4 (CCSM4) (Gent et al., 2011).

ESDD
6, 1395–1443, 2015
An ice sheet model of reduced complexity for paleoclimate studies
B. Neff et al.

Accumulation is the cumulative precipitation below 0 °C. However, the use of daily averages does not account for potentially lower temperatures during the night that may be below freezing. Also, precipitation at temperatures above the melting point might refreeze upon contact with the cold snow surface. Thus, the sensitivity of the accumulation temperature T_{acc} is tested and used to tune the model.

Melting of the ice is parameterized with the positive degree day method (Reeh, 1991). For each grid point, daily average temperatures above 0 °C are integrated over one year to obtain the positive degree days (PDD) as a simplified measure of the energy available for melting. This number is then multiplied with the melting parameter β to calculate the mass loss. β is an empirical constant that accounts for the effect of the local climate and the surface radiation balance. Thus, it is known to largely vary with changing surface conditions, including the density of the surface snow or ice, the presence of meltwater and other effects on the local albedo (Braithwaite, 1995; Charbit et al., 2013). To partially account for these effects, many studies employ two individual melting parameters for snow and bare ice (Huybrechts and T'siobbel, 1995; Huybrechts and de Wolde, 1999). The extent and volume of simulated ice sheets is very sensitive to the choice of melting parameters (Ritz et al., 1997). For the present study, we neglect these complications in spite of their possibly important impact on the sensitivity of the simulated ice sheets. Therefore, only one melting parameter is used for ice. As with the accumulation temperature, the sensitivity of the ice sheet to β is also tested and used for tuning purposes (Table 3).

Climate forcing for preindustrial (PI) and glacial (LGM) climates is provided by simulations with the atmosphere component of CCSM4 (Gent et al., 2011; Neale et al., 2013) (Table 2), which have been analyzed and validated earlier by Hofer et al. (2012) and Merz et al. (2013). The lower boundary conditions for the sea surface are derived from fully-coupled simulations with the preceding model version, CCSM3, as outlined in detail in the original publications. Each CCSM4 simulation ran for 33 years. Climatological daily fields of surface air temperature and total precipitation of the last 30 years

ESDD
6, 1395–1443, 2015

of the simulations are extracted to force the ice sheet model. The spatial resolution is $0.9^\circ \times 1.25^\circ$.

All simulated climate variables are referenced to the continental surface in the relatively coarse grid of the climate model. This does not not concur with the more finely resolved topography of the ice sheet model, in particular since the growth of ice entails considerable changes in the surface elevation. Thus, after a bilinear interpolation from the climate model to the ice sheet model grid, the climatological fields of surface air temperature are corrected for altitude with a constant lapse rate $\Gamma = -6.5 \times 10^{-3}\,\mathrm{K\,m^{-1}}$:

$$T_{\mathrm{ISM}}(t) = T_{\mathrm{GCM}} + \Gamma \cdot (Z_{\mathrm{ISM}}(t) - Z_{\mathrm{GCM}}), \tag{4}$$

where Z_{GCM} is the elevation of the interpolated climate model grid, $Z_{\mathrm{ISM}}(\mathrm{t})$ is the time-dependent elevation of the ice sheet model surface, and analogously for T_{GCM} and $T_{\mathrm{ISM}}(t)$. This correction is applied throughout the ice sheet model simulation to account for changes in ice surface topography.

Precipitation is corrected with a height-desertification effect: values above $Z_0 = 2000\,\mathrm{m}$ are halved every 1000 m (Budd and Smith, 1979). The precipitation rate P_{ISM} at the height of the ice sheet Z_{ISM} is derived from the precipitation of the GCM precipitation P_{GCM} as follows:

$$P_{\mathrm{ISM}} = P_{\mathrm{GCM}} \cdot \exp(-\lambda_{\mathrm{p}}(\max(Z_{\mathrm{ISM}}, Z_0) - \max(Z_{\mathrm{GCM}}, Z_0))) \tag{5}$$

with $\lambda_{\mathrm{p}} = \ln(2)/1000\,\mathrm{m}$. Z_0 refers to the initial surface elevation in the first time step without ice, Z_{GCM} is the surface elevation used in the GCM simulation from the climate input. All used constants are in Table 1.

Comparison of the present day simulation of CCSM4 with reanalyzed data from ERA-Interim (Dee et al., 2011) reveals considerable temperature biases. The CCSM3 simulation which is used as ocean forcing for the CCSM4 simulations overestimates the amount of sea ice in the Northern Hemisphere (Collins et al., 2006), causing too cold temperatures in these areas (Fig. 1). The anomalies range from -12.5 to $+5.5\,^\circ\mathrm{C}$ with an overall average of $-3.0\,^\circ\mathrm{C}$.

To remove this shortcoming of the lower boundary conditions from the simulations, the bias is subtracted from the daily temperature fields after interpolation to the ice sheet grid but before the lapse rate correction. The influence of this correction is investigated by forcing the ice sheet model with both the corrected (LGM_{bs}, bs = bias subtracted) and uncorrected (LGM_{uc}, uc = uncorrected) surface climate fields. The precipitation is not altered in any simulation concerning this temperature bias. But note that the ratio of solid to liquid precipitation of the accumulation is affected by the temperature change.

2.3 Model domain

The domain of the model is limited to the Northern Hemisphere because approximately 80 % of the changes in ice volume during the LGM took place on the Northern Hemisphere (Clark and Mix, 2002). A polar azimuthal projection is used as grid base. The lateral grid is identical to the one of SICOPOLIS (Greve, 1997; Born et al., 2010).

The spatial resolution is 40 km × 40 km. Each grid cell has exactly one vertical layer which stores all information such as ice thickness, accumulation, ablation. An ice mask is introduced to reduce cost-intensive ice flux calculations to grid cells with ice instead of the entire model domain. The temporal resolution is one year which makes it impossible to implement a seasonal cycle in the SMB.

The SMB of the Himalayas is not well represented in the current model version. The simplified ablation scheme does not explicitly account for melting by shortwave radiation at subzero temperatures and large intra-day and intra-seasonal variations in both accumulation and melting. Both effects are more important at the subtropical latitude of the Himalayas than further north where glacier growth and decay are confined to two individual seasons. Thus, in the Himalayas, the approach used here leads to an unrealistically high accumulation rate, which destabilizes the model. For this reason, the accumulation in this region is set to zero.

ESDD
6, 1395–1443, 2015

Sea level

The changing sea level during the simulations has a large influence on the ice flow, since some shallow bays fall dry and provide the possibility for the ice to cover new areas, for example the Baltic Sea or the Great Banks off Newfoundland.

All simulations start without any ice in the Northern Hemisphere which leads to an offset in sea level compared to today's situation. This offset of 7.36 m (Table 1) is equivalent to the ice volume on Greenland, the major storage in the Northern Hemisphere, would melt (Bamber et al., 2013). The change of the global mean sea level is retrieved by dividing the water equivalent of the total ice volume by the ocean area of $3.625 \times 10^{14}\,\mathrm{m}^2$ (IPCC, 2007). All ice volumes in this work are presented as sea level equivalent (SLE). The initial positive offset from Greenland of 7.36 m is added to all sea levels, therefore, an ice-free Northern Hemisphere is not equal to 0 m SLE.

Ice shelves are not simulated. Ice is assumed to calve into the ocean upon contact with the shoreline, approximated by setting the ice thickness to zero at these points. This may yield to less ice in the coastal areas for neglecting the buttressing effect of ice shelves (Dupont and Alley, 2005). However, to avoid overly rapid ice loss due to rising sea level, already existing ice is allowed to persist unless it starts to float. If the existing ice column with a density of $910\,\mathrm{kg\,m^{-3}}$ is able to displace the water column between the bedrock and sea level, i.e., the hydrostatic equilibrium is not yet reached, the ice is still treated as grounded and the grid point is equivalent to land. As soon as the mass of the water column exceeds the ice mass, all ice is removed and the grid cell is converted to a water cell.

3 Test cases on a square domain

In order to test the present model formulation, we perform a series of benchmark experiments defined by the European Ice Sheet Modelling INiTiative (EISMINT) (Huy-

ESDD
6, 1395–1443, 2015

brechts et al., 1996). To validate our model and their results, both the fixed-margin ($\mathrm{EISMINT_{fixed}}$) and moving-margin ($\mathrm{EISMINT_{freemargin}}$) experiments are carried out.

$\mathrm{EISMINT_{fixed}}$ uses a flat bed without relaxation. It prescribes a constant SMB of $0.3\,\mathrm{m\,yr^{-1}}$ in the entire domain. The shape of the simulated ice sheet is symmetric, ruling out inconsistencies in the grid configuration (Fig. 2, left). Our experiment $\mathrm{EISMINT_{fixed}}$ is indistinguishable from the reference (Huybrechts et al., 1996). Both peaks in the center of the area are 3342.6 m above ground.

The second benchmark $\mathrm{EISMINT_{freemargin}}$ also uses a flat rigid bed. Here, the SMB linearly decreases from the center of the grid toward the boundaries. This pattern is point-symmetric around the central point so that the SMB function resembles an upright cone. Thus, the IceBern2D simulation is also symmetric with respect to the center of the model domain (Fig. 2, right). Again, we find very close agreement with the results of Huybrechts et al. (1996), with a deviation of less than 1 % in the elevation of the central peak. This confirms the validity of the formulation and implementation of the IceBern2D model. In the next section we apply our model to climatically relevant configurations and conditions.

4 Northern Hemisphere ice volume in preindustrial and glacial climates

4.1 Last glacial maximum climate forcing, model tuning

The sensitivity of the IceBern2D model to four empirical model parameters is investigated by varying their values within their range of uncertainty (Table 3). There are two parameters that change the surface mass balance (SMB): the melting parameter β and the accumulation temperature T_{acc}. The other two influence the ice flow. The flow enhancement parameter E linearly modifies the flow-law parameter A (Eq. 2). τ_{br} determines the relaxation time of the bedrock which influences the ice flow. If the bedrock stays longer at its initial elevation, the elevation gradient ∇Z is higher (Eq. 2). The bedrock relaxation τ_{br} also has an indirect influence on the SMB. The elevation and

ESDD
6, 1395–1443, 2015

therefore the temperature decreases at the surface when the elevation yields under the ice. A shorter relaxation time leads to a decrease of the SMB. All possible parameter perturbations amount to a total of 200 combinations. Each simulation is forced with the two versions of LGM forcing outlined above.

This large number of simulations is evaluated primarily by their simulated total ice volume which is compared to available reconstructions (Denton, 1981; Peltier, 2002; Clark and Mix, 2002; Peltier, 2004). Although the ice sheets in the LGM were not in equilibrium (Clark et al., 2009; Heinemann et al., 2014), the simulations here are forced with an LGM climate until equilibrium is reached. Therefore, the ice volume may differ in the simulations compared to LGM reconstructions.

The spread of the ice volume in sea level equivalent (SLE) depends significantly on the climate forcing. For the climate forcing without temperature bias correction (LGM_{uc}), the spread of the ice volume is between −270 and −65 m SLE, while the spread for the bias corrected climate forcing (LGM_{bs}) is much smaller between −130 and −65 m (Fig. 4, lower part).

Each tuning parameter (Table 3) has different influences on the maximum volume. Figure 3 illustrates the tendency and distribution of these tuning parameters. The melting parameter β has the strongest influence on ice volume in comparison with other parameters. The mean sea level, as well as the the 95 percentile, decrease with increases in β. This variation between different values of β is also seen in the other diagrams, where different values of β are shown as columns of dots. Generally, the width of the distribution also decreases with increasing β. A large jump in SLE is observed between 6 and 7 mm PDD^{-1} which is also visible in the density distribution (Fig. 4, lower part). Simulations with an ice volume above 200 m SLE tend to have a β lower or equal than 7 mm PDD^{-1} with three exceptions.

Compared to the impact of β and the climate boundary conditions, the influence of all other model parameters on ice volume is relatively weak. A weak influence of the flow enhancement parameter E to maximum ice volume is apparent as faster ice flux leads to lower ice volumes. The lower bound increases faster with larger E while

ESDD
6, 1395–1443, 2015

the upper limit is almost fixed. Therefore, the group of isolated ensemble members with a low β at the upper limit gets closer to the mean values. The mean and median are closer at a higher ice flux. The influence of the accumulation temperature T_{acc} on minimum sea level is very small. Higher T_{acc} results in a slightly lower sea level, because it leads to more accumulation. No apparent difference is visible between the two bedrock relaxation time scales τ_{br}. This result is not unexpected because τ_{br} only impacts the transient bedrock sinking during the ice sheet build-up, not the maximum ice volume shown here. The median, mean and also the percentile boxes are similar for both bedrock relaxation times.

Figure 4 is separated into two parts. Both share the horizontal axis that represents the total ice volume in SLE. The upper part is a tree plot, where each layer represents one specific tuning parameter to illustrate the spread they cause. At the bottom all individual simulations are shown. From bottom to top, simulations are averaged parameter-wise at each level. Thus, the ice volume range caused by variations in each individual tuning parameter is visualized by the divergent lines from the top down. The highest point is the average of all ensemble simulations. The two ensembles are shown in different colors as before. As an example, each of the twenty points of one climate forcing at the third layer from the top represent the average of all combinations of T_{acc} and τ_{br}. As this level illustrates the impact of E, four points representing the different considered values of this variable connect into one single dot at their average position of the level above. This yields five different dots, each representing one of the possible values of β. For better readability, the parameters have been ordered so that the one with the greatest influence on minimum ice volume is on top (β) and the least sensitive at the bottom (τ_{br}). With the information about the tendency of the sea level change with respect to the parameter variations (Fig. 3) it is possible to address the individual values (Table 3) at each parameter branch. The lower part of this figure shows a density distribution of the sea level for each climate forcing. It is consistent with the points of the last row in the upper part and distributes these among 100 classes over the whole bandwidth.

ESDD
6, 1395–1443, 2015

The tree plot shows that the influence of the tuning parameter has a clear order. Nevertheless, there are a few obvious examples, where the points change the position and join a cluster of another branch. The most prominent example are six simulations with different bedrock relaxations which have a gap of more than 80 m SLE and each of them is positioned exactly on one side of the big split. A Longer relaxation time leads to larger ice volumes, because ice sheets can grow faster with a long relaxation time and may stabilize at this larger volume because the surface elevation remains longer at high altitudes with positive SMB.

The density distribution shows a non-normal distribution for every ensemble of different climate forcing. LGM_{uc} has two obvious groups with a gap of roughly 50 m SLE. The group with the lower sea level consists of β configurations with 5 and 6 mm PDD^{-1} (see Fig. 3), the group with the upper sea level includes all β greater and equal than 7 mm PDD^{-1}. Responsible for this gap is the Laurentide ice sheet. During the build-up process of the Laurentide ice sheet the eastern and western ice streams join together to a single ice body. Simulations in the LGM_{uc} ensemble with an ice volume greater than 225 SLE consist of a single Laurentide ice sheet, while simulations with a lower ice volume these two streams are not in contact with each other. The LGM_{bs} is also separated into two groups but the width of the gap is only around 10 m SLE. Again, the two groups are mostly defined by different values of β and the connection of the eastern and western ice stream to the Laurentide ice sheet.

Figure 4 highlights potential LGM ice volumes (Clark and Mix, 2002) as gray horizontal bars in the density distribution. The lower limit at −95 m SLE is mainly from Peltier (2002) while the upper limit at −132 m SLE corresponds to the maximum CLIMAP reconstruction (Denton, 1981) for the Northern Hemisphere in each case. The ICE-5G reconstruction from Peltier (2004) with −117 m SLE is located in the center of the bar. Simulations below this bar are considered as suitable LGM simulations for further investigations. The LGM_{uc} ensemble has 50 possible LGM simulations while from LGM_{bs} climate forcing 114 simulations are considered. The averages of these simulations for

ESDD
6, 1395–1443, 2015

each respective climate forcing look quite different (Fig. 5) although these two ensemble composites differ in their ice volume by only 3 m SLE.

The most obvious difference between the two composites is the Laurentide ice sheet. The ice flows from two different streams towards the Great Plains. With the LGM_{uc} forcing, these two streams are not connected in any simulation. A gap in the Great Plains remains. This is due to higher temperatures in the Great Plains in the LGM_{uc} ensemble than in the corrected version (Fig. 1). Therefore, with LGM_{bs} forcing, eastern and western Laurentide ice streams connect easier and faster compared to the uncorrected ensemble but the two domes remain separated. This is consistent with the ICE-5G reconstruction that also suggests two distinct domes on the Laurentide ice sheet (Fig. 6, right). However, the separation is probably exaggerated in our simulations because the Hudson Bay remains below sea level and therefore ice-free.

The Eurasian ice sheet accumulates in the LGM_{bs} less ice compared to the uncorrected version. The British Isles and Scandinavia are covered by ice in both ensembles. The Eurasian ice sheet in the LGM_{uc} ensemble without the temperature bias correction consists of one large ice sheet with a connected and distinct eastern part. Whereas the ensemble LGM_{bs} has two individual small Eurasian ice sheets of almost equal expansion. The model accumulates ice in the Alps in both ensembles which are discrete from other ice masses. The LGM_{uc} accumulates more ice in Eurasia and is therefore closer to ICE-5G. Nevertheless, both climate forcing underestimate the ice volume in Eurasia.

The Bering Strait and the Asian far east region in LGM_{bs} ensemble are similar to the ICE-5G reconstruction (Fig. 6, right). The LGM_{uc} ensemble accumulates ice in the American part of the Bering Strait, whereas the ice in the LGM_{bs} ensemble and ICE-5G reconstruction is in this part not that distinct. Ziemen et al. (2014) attributes the overestimated accumulation in this region to the missing albedo variation in their model and moisture blocking of the atmospheric forcing. The land around the New Siberian Islands is covered by a small ice sheet in both ensembles while this area is ice free in the LGM ICE-5G reconstruction.

ESDD
6, 1395–1443, 2015

Overall, the results with LGM_{bs} forcing are closer to the LGM reconstruction. Besides the relatively small Eurasian ice sheet, the ice distribution is closer to ICE-5G in all considered LGM_{bs} ensemble members than the ones from the LGM_{uc} ensemble. The spread of the minimum sea level (Fig. 3) is narrow and more than half of all LGM_{bs} simulations are considered valid in terms of minimum LGM sea level compared to only one quarter of all LGM_{uc} simulations. Therefore, only ensemble LGM_{uc} is not further considered in the results section.

Table 4 shows the distribution of all tuning parameters from all 114 LGM_{bs} simulations with an ice volume between 95 and 132 m SLE (see Fig. 4). These simulations constitute the ensemble composite from Fig. 5 (right). The distribution of β has a clear peak at 6 mm PDD^{-1} very close to the average of 5.97 mm PDD^{-1}. For the flow enhancement factor E, most simulations consistent with reconstructions have values of 75 and 100 % with an average of 111 %. The accumulation temperature A_{temp} shows a slight tendency to warmer temperatures and the two bedrock relaxations τ_{br} are distributed almost equally.

Representing the average over a large number of potentially very different simulations of ice distribution with different model parameters, the composites are not physically consistent. Thus, the composite for LGM_{bs} is now compared with the equilibrium state of the simulation whose parameters are closest to the mean value of the parameters of the ensemble composite (β = 6 mm PDD^{-1}, E = 100 %, T_{acc} = 2 °C, τ_{br} = 3000 yr; Table 4). The situation in Eurasia, Greenland and Bering Strait is very similar between this simulation (Fig. 6, left) and the ensemble composite (Fig. 5, right). Nevertheless, there are small differences at the Laurentide ice sheet between these two results. The single simulation consistent with the approximate mean values shows indications of a single dome Laurentide ice sheet, whereas the two individual domes that merge to form the Laurentide ice sheet, consistent with reconstructions (Stokes et al., 2012; Kleman et al., 2013), are still visible in the ensemble composite. Both the single simulation and the ensemble composite have a very similar total ice volume of approximately 115 m SLE. However, the former is in overall better agreement with

ESDD
6, 1395–1443, 2015

ICE-5G from Peltier (2004). Therefore, this parameter set is considered as the best-guess tuning parameters (Table 1). For further investigations, only this parameter set is considered.

Simulations at the upper limit of the LGM sea level at 130 m SLE have a similar ice distribution in Eurasia as the simulation with the best guess tuning parameters (not shown). The additional ice volume is mainly due to thicker ice in the same regions as in Fig. 6 (left) and does not add to the ice sheet area. All simulations with realistic LGM sea level underestimate the Eurasian ice sheet.

4.2 Preindustrial climate forcing

The IceBern2D is strongly dependent on the surface mass balance (SMB) and the tuning parameters β and T_{acc} directly related to it. To benchmark the best-guess tuning parameters (values in Table 1) from the $\mathrm{LGM_{bs}}$ simulation, IceBern2D is applied on the Northern Hemisphere under preindustrial conditions (Table 2).

Both versions of preindustrial forcing without the temperature bias ($\mathrm{PI_{uc}}$ and $\mathrm{PI_{bs}}$) do not accumulate significant ice volumes in the Northern Hemisphere (Fig. 7) with the best-guess tuning parameters ($\beta = 6\,\mathrm{mm\,PDD^{-1}}$, $T_{\mathrm{acc}} = 2\,^{\circ}\mathrm{C}$, $E = 100\,\%$ and $\tau = 3000\,\mathrm{yr}$). The ice volumes correspond to -8.2 m SLE and -4.1 m SLE, respectively, with the most suitable tuning parameters where the positive offset of 7.36 m SLE from Greenland is already subtracted from the values. The most conspicuous difference between the two climate forcings is on Baffin Islands and Chukotka in far eastern Siberia. The forcing without the temperature bias ($\mathrm{PI_{bs}}$) accumulates much less ice in this area, and the result is more realistic. Both climate forcings result in very similar ice volume of Greenland with 10.0 m SLE ($\mathrm{PI_{uc}}$) and 9.9 m SLE ($\mathrm{PI_{bs}}$). This exceeds the ice volume of ETOPO1 (Amante and Eakins, 2009) by 3 m SLE.

ESDD
6, 1395–1443, 2015

4.3 Multiple equilibria in Northern Hemisphere ice volume

One of the primary advantages of the ice sheet model is its computational efficiency and hence the possibility for large ensemble simulations and long integration times. Here, a reduced ensemble of 18 parameter combinations (Table 5) has been forced with the LGM_{bs} data and a slowly varying global temperature offset. Temperature anomalies have been linearly decreased from +5 to −5 °C over 2.5 million years and increased again to +5 °C in the same way. The maximum temperature offset corresponds to the temperature difference between the CCSM4 LGM and PI simulation of 4.97 K in the Northern Hemisphere (Table 2). One simulation had numerical instabilities after 4.5 mio years and was not considered in the results.

To ensure that the rate of temperature change is slow enough for the ice sheet to remain in continuous quasi-equilibrium, seven simulations were carried out with the best-guess parameter set in which the temperature change was interrupted at different values. These simulations continued with a constant temperature offset for 100 000 years (Fig. 8, black dots on the right). These interrupted runs confirm that the transient simulation is a good approximation to a continuous equilibrium.

The ice volume as a function of the temperature offset describes a hysteresis (Fig. 8). There are two stable equilibria for almost every temperature, depending on the initial value of the ice volume. This is valid globally as well as for the individual regions North America and Eurasia (Fig. 8c and d). In contrast to the global ice volumes (a,b), the regional ice volumes in Fig. 8c and d have no global sea level offset of 7.36 m.

Different tuning parameters have a modest influence on the overall shape of the hysteresis and major transitions (Fig. 8a). A slight horizontal shift to a later or earlier ice volume change is visible. Simulations with the same melting parameter β are close together and identify as three individual groups at the build up of the ice sheet. All 6 simulations with a β of 5 mm PDD^{-1} reach ice volumes greater than 500 m SLE and are not in equilibrium at the cold extreme of the forcing range. The reason for this additional ice growth is a large region in Central Siberia where SMB becomes positive. This

ESDD
6, 1395–1443, 2015
An ice sheet model of reduced complexity for paleoclimate studies
B. Neff et al.

illustrates that the open southern boundaries on both major land masses complicate the definition of the hysteresis loop, because the upper limit is not limited by continental boundaries. Nevertheless, the evolution of all ensemble members is similar, which justifies to limit the detailed discussion to the single hysteresis simulations with the best-guess parameter set (Fig. 8b–d)

There are three processes which influence rapid ice volume changes. They can be seen in the hysteresis (Fig. 8) as an almost vertical volume change. The most important influence is the positive ice elevation feedback. As soon as the surface temperature reaches a certain level where the SMB turns positive, the ice sheet grows fast to higher and colder elevations and stabilizes itself. Adjacent areas may be influenced by the ice flow from these newly glaciated regions, so that the SMB turns positive there too. A positive feedback is induced which is much faster compared to the temperature change of the hysteresis (Fig. 8c, at 2 °C).

Another strong influence during the build up process on the ice volume is the contact of two individual ice sheets over eastern and western North America that combine to form the Laurentide ice sheet. Although we use an idealized forcing, this evolution is consistent with reconstructions of the last glaciation (Stokes et al., 2012; Kleman et al., 2013). The ice volume increases considerably as soon as these two streams connect with each other (Fig. 8c, at 0.5 °C) because ice flows from two different directions into the center of the continent. The connection of these two streams is responsible for the jump of roughly 40 m SLE. The ice volume in North America decreases steadily and relatively slowly on the descending branch of the hysteresis until a positive temperature offset of 3 °C. At higher temperatures the SMB turns positive in the southern part of the central Laurentide ice sheet and it retreats quickly, especially the western part disappears almost completely. The eastern part is not in equilibrium with the underlying bedrock after this rapid ice loss. Therefore a small rebound of the ice volume is visible after the ice volume decrease of almost 100 m SLE (Fig. 8c).

The sea level change due to formation of ice on land has an important indirect influence on the ice distribution especially in Europe. Ice sheets isolated by water masses,

ESDD
6, 1395–1443, 2015

ie. British Isles or Scandinavia, are not able to bypass these barriers because the Ice-Bern2D does not include floating ice shelves. However, if the water level drops below a certain level, areas previously separated by water join and ice can expand into new regions. The sea level change may have an immediate effect if the ice sheet is already in contact with the water barrier and can expand in regions that fall dry, e.g., the Great Banks of Newfoundland.

At the beginning of the hysteresis, at temperatures above 2.5 °C, the Northern Hemisphere apart from Greenland is nearly ice free. After one complete hysteresis loop, most of the simulations reach a similar ice volume at the initial temperature offset of $\Delta + 5$ °C than at the ice free beginning. However, the simulation with the best-guess parameter set does not become ice-free at the end of the hysteresis. Especially the Laurentide ice sheet has still some remarkable volume while the Eurasian ice sheet disappears around 4 °C (Fig. 8c and d).

The difference in ice volume between the ascending and descending branches of the hysteresis at a temperature offset of $\Delta T = 0$ °C, i.e., with the $\mathrm{LGM_{bs}}$ forcing, is 123 m SLE. The shape and distribution of the simulated ice sheets on the lower branch of the hysteresis after 1.25 mio years is virtually indistinguishable from the equilibrium of the simulations with constant forcing shown in Sect. 4.1 (Fig. 6, left). Figure 9 shows the ice thickness for $\Delta T = 0$ °C after 3.75 mio years on the upper branch of the hysteresis. All ice masses but Greenland are considerably larger, amounting to about 50 m SLE on North America alone. The extent of the Laurentide ice sheet is mostly the same as on the lower branch of the hysteresis as it does not extend further south. The only major difference in ice are is the fully ice-covered Hudson Bay due to the intermittently lower sea level. The ice volume difference in Eurasia is roughly 40 m SLE, but during the build up process Eurasia is nearly ice free. Therefore, the relative difference volume of the hysteresis in Eurasian ice is very large (Fig. 8d). At the LGM temperature $\Delta T = 0$ °C on the lower branch, only two small ice sheets are present on Scandinavia and the British Isles. On the upper branch, the Eurasian ice sheet stretches all the way from the British Isles to far eastern Siberia. The constant climate forcing is unrealis-

ESDD
6, 1395–1443, 2015

tic for the last glaciation and could explain the underrepresented Eurasian ice sheet from the LGM simulations above. Therefore, small temperature or precipitation variations could lead to higher ice masses in Eurasia similar in result to the idealized forcing that causes the hysteresis. This latter simulation resembles the ICE-5G reconstruction more closely (Figs. 9 and 6, right). The additional 30 m SLE of ice to explain the lower to upper hysteresis difference at $\Delta T = 0\,^{\circ}\mathrm{C}$ are found in Siberia which but outside the region that was covered by the Eurasian ice sheet in reconstructions (see Fig. 9) (Svendsen et al., 2004). At the same temperature offset, this area is nearly ice free on the lower branch of the hysteresis.

5 Summary and discussion

In this study, we present a model for continental-scale ice sheets that simplifies the dynamics of ice flow into a single, vertically integrated layer. The resulting two-dimensional flow is simulated on a rectangular domain that covers most of the land mass of the Northern Hemisphere. The surface mass balance uses the positive degree day method (Reeh, 1991), based on daily fields of surface air temperature and total precipitation from the comprehensive global climate model CESM1 (Gent et al., 2011; Merz et al., 2013). Eustatic sea level and the land mask are prognostically adjusted as a function of the simulated ice volume.

The simplified dynamics of the ice flow compare favorably in the standardized tests of the EISMINT project (Huybrechts et al., 1996).

Similar models have been used to study the last glacial inception in Europe (Oerlemans, 1981a; Siegert et al., 1999) and the sensitivity of climate-ice sheet interactions during the last glacial cycle (Neeman et al., 1988). Strong adaptations in the present day climate (Siegert and Marsiat, 2001) were necessary to get similar results as LGM reconstructions from Svendsen et al. (2004). However, existing ice sheet models of reduced complexity applied to small regional scales (Näslund et al., 2003) or on a semi-hemispheric coarse grid (Neeman et al., 1988) showed adequate results. Nevertheless, simulations on a fine grid over the Northern Hemisphere with a precise bedrock and its relaxation have until now not been carried out with a 2D shallow ice approximation model.

Taking advantage of the computational efficiency of the model, a large set of simulations with perturbed parameters is used to optimize the simulation of Northern Hemisphere ice volume during the Last Glacial Maximum (Peltier, 2004). Results show a reasonable agreement on North America, while the Eurasian ice sheet is too small. This is likely due to the lack of ice shelves in our model that does not allow the Barents Sea to be covered by ice and delays the development of an ice sheet on the Baltic and North Seas until the sea level is low enough for grounded ice to locally grow or advance into the area. This could be a problem as the marine ice sheets of the Barents and Kara Seas have been shown to play a pivotal role early during the last glaciation (Svendsen et al., 2004). On regional scales the missing ice shelf may influence the results, ie. the Hudson Bay would be covered by shelf ice wile it remains ice free in IceBern2D LGM simulations. Furthermore, ice shelves buttress the ice sheet flow (Dupont and Alley, 2005). While the fundamentally different stress balance of ice shelves cannot be included in our model at this point, one possible solution is to allow the grounded ice to grow into deep water down to a certain water depth (Siegert et al., 1999; Tarasov and Peltier, 1999; Abe-Ouchi et al., 2013). Aside from these shortcomings, the optimized model version yields a realistic modern ice distribution when forced with simulated preindustrial climate from the same model.

The overestimated sea ice in the CCSM simulations (Collins et al., 2006) and the associated temperature bias influences the global ice sheet volume and its distribution. Simulations forced with the colder uncorrected climate (LGM_{uc}) have a lower and a wider distribution of the ice volume. The temperature of the corrected ensemble (LGM_{bs}) is on average 3 °C warmer. The simulated density distribution of ice volumes is therefore limited to a smaller bandwidth of a 3 °C warmer climate with an ice free Northern Hemisphere as the lower limit. Local temperature corrections in the LGM_{bs}

ESDD
6, 1395–1443, 2015

ensemble overall lead to results which are comparable to LGM reconstructions as ICE-5G.

Although the LGM ice sheet was not in equilibrium (Clark et al., 2009; Heinemann et al., 2014), all simulations are forced until an equilibrium is achieved. It takes around 120 kyr years with a constant climate forcing until a steady state of all ice sheets is reached. LGM cycles in the past 500 kyr years are around 100 kyr years (Hays et al., 1976; Imbrie and Imbrie, 1980), nevertheless, cycles between 80 and 120 kyr are not unusual (Huybers and Wunsch, 2005). During LGM the Laurentide ice sheet was known to be dry (Bromwich et al., 2004), therefore, a constant LGM climate forcing beginning at an ice free hemisphere takes longer to establish a full grown Laurentide ice sheet.

Owing to the focus on simplicity and numerical efficiency, the thermal coupling of the ice dynamics as well as basal melting are neglected. However, Calov and Marsiat (1998) showed that vertically integrated models yield results of comparable quality as thermomechanical models. They also conclude that the representation of SMB is more important to simulate the last glacial cycle than the accurate description of ice dynamics. Nevertheless, Johnson and Fastook (2002) state, that basal melting can have a dramatic effect on the glaciation cycle. It is theoretically possible to approximate melting at the bottom of the ice sheet by a function based on accumulation rate, temperature and geothermal heat flux. However, this could be the subject of further model development.

In long simulations we find multiple equilibria in ice volume, as evidenced by the hysteresis. A global temperature offset is applied to the $\mathrm{LGM_{bs}}$ forcing. Starting at $+5\,^{\circ}\mathrm{C}$, approximately the difference between the simulated LGM and preindustrial climates in CESM in the ice sheet model domain, the offset linearly decreases to $-5\,^{\circ}\mathrm{C}$ over the course of 2.5 million years. The very slow transient temperature change ensures that the simulated ice sheet remains in continuous quasi-equilibrium. Subsequently, temperature is increased slowly back to $+5\,^{\circ}\mathrm{C}$. Both the North American and Eurasian ice

ESDD
6, 1395–1443, 2015

sheets are found to have at least two stable states over almost the entire temperature offset range.

Ice volume increases and decreases abruptly at several points on the temperature scale. As soon as temperatures are low enough for the local mass balance to become positive, the ice sheet quickly grows to higher, colder elevations and thereby stabilizes itself. This mechanism is consistent with similar simulations of the Cenozoic Antarctic Ice Sheet (Pollard and DeConto, 2005). Importantly, the individual jumps in ice volume depend on the local mass balance and the ice sheet geometry alone, which both are closely related to the bed topography. Variations in the model parameters play a secondary role as they may shift these glaciation and deglaciation events on the temperature scale but do not affect their existence or individual height.

Our hysteresis experiments are similar to simulations by Abe-Ouchi et al. (2013), although they employed more comprehensive representations for both climate variations and ice sheet dynamics, and consequentially cannot continuously vary temperature offsets. We confirm that the hysteresis of the North American ice sheet is located at warmer temperature offsets than the hysteresis of the Eurasian ice sheet. Also, the retreating North American ice sheet is most sensitive to temperature increase when its volume is between 120 and 50 m SLE. Disagreement is found for the Eurasian ice sheet, as our model does not find a rapid retreat for rising temperatures. The simulated volume is generally lower here. This is likely due to the inadequate representation of marine ice sheets in our model.

The insufficient glaciation over Northern Europe shelf seas and the correct LGM ice volume over Eurasia may be recovered if the model is initialized with an ice covered state like on the descending branch of the hysteresis. Initialization with a large global ice volume and corresponding low sea level allows ice to cover shelf seas and to grow thicker and more stable. However, the simple hysteresis initialization yields a ice volume of 45 m SLE for the Eurasian ice sheet, considerably more than the 13–25 m SLE in reconstructions (Clark and Mix, 2002). Note that this effect somewhat undermines the ensemble optimization that targets the LGM total ice volume but only considers the initialization without ice.

6 Conclusions and outlook

Ice sheet models of reduced complexity may complement comprehensive models of ice dynamics and thus close the gap that exists for climate simulations over many glacial cycles and over the next centuries to millennia. Their computational efficiency enables research questions that are not primarily concerned with the detailed stress balance inside the ice but rather benefit from a more detailed representation of the surface mass balance, a better coupling with the climate system, probabilistic analyses based on multiple simulations and parameter perturbations, or extremely long integration times. Several of these points arguably apply to the uncertainties and remaining questions related to the succession of ice ages over the last million years. One recent example are simulations of the Eemian interglacial. Although different studies used models with a similar three-dimensional representation of ice dynamics, in some cases even the same model, the simulations of the Eemian minimum ice volume over Greenland diverge widely (Fig. 5.16 in Masson-Delmotte et al., 2013), probably due to the different representations of the climate forcing and the surface mass and energy balances (Robinson et al., 2011; Born and Nisancioglu, 2012; Quiquet et al., 2013; Stone et al., 2013).

We conclude that our model achieves a reasonable agreement for the ice distribution and volume of the Last Glacial Maximum and today in spite of its simplicity. Future simulations will benefit from a comprehensive surface mass and energy balance model (Greuell and Konzelmann, 1994; Reijmer and Hock, 2008) that is currently being adapted for use over millennial time scales. This will allow a fully bi-directional coupling of the ice sheet model with the Bern3D climate model (Ritz et al., 2011).

Investigations of climate change on orbital time scales have in the past been limited by computational constraints to statistical (Raymo and Nisancioglu, 2003; Huybers,

Discussion Paper | Discussion Paper | Discussion Paper | Discussion Paper |

ESDD

6, 1395–1443, 2015

An ice sheet model of reduced complexity for paleoclimate studies

B. Neff et al.

2006) or conceptual models (Paillard, 1998). The present study represents a first step toward a fully integrated earth system model to address questions based on appropriate Earth System models.

Acknowledgements. A. Born acknowledges financial support from the European Commission under the Marie Curie Intra-European Fellowship ECLIPS (PIEF-GA-2011-300544). T. F. Stocker received support from the Swiss National Science Foundation.

References

Abe-Ouchi, A., Saito, F., Kawamura, K., Raymo, M. E., Okuno, J., Takahashi, K., and Blatter, H.:Insolation-driven 100,000-year glacial cycles and hysteresis of ice-sheet volume, Nature, 500, 190–193, doi:10.1038/nature12374, 2013. 1398, 1417, 1419

Amante, C. and Eakins, B. W.: ETOPO1 1 Arc-Minute Global Relief Model: Procedures, Data Sources and Analysis, NOAA Technical Memorandum NESDIS NGDC-24, National Geophysical Data Center, NOAA, doi:10.7289/V5C8276M, 2009. 1401, 1412

Arakawa, A. and Lamb, V. R.: Computational design of the basic dynamical processes of the UCLA general circulation model, Meth. Comp. Phys., 17, 173–265, 1977. 1399

Archer, D., Winguth, A., Lea, D., and Mahowald, N.: What caused the glacial/interglacial atmospheric pCO2 cycles?, Rev. Geophys., 38, 159–189, doi:10.1029/1999RG000066, 2000. 1397

Bamber, J. L., Griggs, J. A., Hurkmans, R. T. W. L., Dowdeswell, J. A., Gogineni, S. P., Howat, I., Mouginot, J., Paden, J., Palmer, S., Rignot, E., and Steinhage, D.: A new bed elevation dataset for Greenland, The Cryosphere, 7, 499–510, doi:10.5194/tc-7-499-2013, 2013. 1405, 1430

Berger, A.: Long-term variations of caloric insolation resulting from the Earth's orbital elements, Quaternary Res., 9, 139–167, 1978. 1397, 1431

Bonelli, S., Charbit, S., Kageyama, M., Woillez, M.-N., Ramstein, G., Dumas, C., and Quiquet, A.: Investigating the evolution of major Northern Hemisphere ice sheets during the last glacial-interglacial cycle, Clim. Past, 5, 329–345, doi:10.5194/cp-5-329-2009, 2009. 1398

Born, A. and Nisancioglu, K. H.: Melting of Northern Greenland during the last interglaciation, The Cryosphere, 6, 1239–1250, doi:10.5194/tc-6-1239-2012, 2012. 1420

ESDD
6, 1395–1443, 2015

Born, A., Kageyama, M., and Nisancioglu, K. H.: Warm Nordic Seas delayed glacial inception in Scandinavia, Clim. Past, 6, 817–826, doi:10.5194/cp-6-817-2010, 2010. 1404
Braithwaite, R. J.: Positive degree-day factors for ablation on the Greenland ice sheet studied by energy-balance modelling, J. Glaciol., 41, 153–160, eng, 1995. 1402
Bromwich, D. H., Toracinta, E. R., Wei, H., Oglesby, R. J., Fastook, J. L., and Hughes, T. J.: Polar MM5 Simulations of the Winter Climate of the Laurentide Ice Sheet at the LGM*, J. Climate, 17, 3415–3433, 2004. 1418
Budd, W. F. and Smith, I. N.: Sea level, ice, and climatic change, in: The growth and retreat of ice sheets in response to orbital radiation changes, edited by: Allison, I., International Association of Hydrological Sciences 1981, London, Oxford, Worcester, 131, 369–409, 1979. 1403, 1430
Calov, R. and Marsiat, I.: Simulations of the Northern Hemisphere through the last glacial-interglacial cycle with a vertically integrated and a three-dimensional thermomechanical ice-sheet model coupled to a climate model, Ann. Glaciol., 27, 169–176, 1998. 1398, 1418
Cess, R. D., Potter, G. L., Zhang, M.-H., Blanchet, J.-P., Chalita, S., Colman, R., Dazlich, D. A., Genio, A. D. D., Dymnikov, V., Galin, V., Jerrett, D., Keup, E., Lacis, A. A., Le Treut, H., Liang, X.-Z., Mahfouf, J.-F., Mcavaney, B. J., Meleshko, V. P., Mitchell, J. F. B., Morcrette, J.-J., Norris, P. M., Randall, D. A., Rikus, L., Roeckner, E., Royer, J.-F., Schlese, U., Sheinin, D. A., Slingo, J. M., Sokolov, A. S., Taylor, K. E., Washington, W. M., Wetherald, R. T., and Yagai, I.: Interpretation of snow-climate feedback as produced by 17 general circulation models, Science, 253, 888–892, doi:10.1126/science.253.5022.888, 1991. 1397
Charbit, S., Ritz, C., Philippon, G., Peyaud, V., and Kageyama, M.: Numerical reconstructions of the Northern Hemisphere ice sheets through the last glacial-interglacial cycle, Clim. Past, 3, 15–37, doi:10.5194/cp-3-15-2007, 2007. 1398
Charbit, S., Dumas, C., Kageyama, M., Roche, D. M., and Ritz, C.: Influence of ablation-related processes in the build-up of simulated Northern Hemisphere ice sheets during the last glacial cycle, The Cryosphere, 7, 681–698, doi:10.5194/tc-7-681-2013, 2013. 1402
Clark, P. U. and Mix, A. C.: Ice sheets and sea level of the Last Glacial Maximum, Quaternary Sci. Rev., 21, 1–7, doi:10.1016/S0277-3791(01)00118-4, 2002. 1404, 1407, 1409, 1419, 1438, 1439
Clark, P. U., Dyke, A. S., Shakun, J. D., Carlson, A. E., Clark, J., Wohlfarth, B., Mitrovica, J. X., Hostetler, S. W., and McCabe, A. M.: The last glacial maximum, Science, 325, 710–714, doi:10.1126/science.1172873, 2009. 1407, 1418

Collins, W. D., Bitz, C. M., Blackmon, M. L., Bonan, G. B., Bretherton, C. S., Carton, J. A., Chang, P., Doney, S. C., Hack, J. J., Henderson, T. B., J. T. Kiehl, W. G. Large, D. S. McKenna, B. D. Santer, and R. D. Smith: The Community Climate System Model version 3 (CCSM3), J. Climate, 19, 2122–2143, doi:10.1175/JCLI3761.1, 2006. 1403, 1417

Dee, D. P., Uppala, S. M., Simmons, A. J., Berrisford, P., Poli, P., Kobayashi, S., Andrae, U., Balmaseda, M. A., Balsamo, G., Bauer, P., Bechtold, P., Beljaars, A. C. M., van de Berg, L., Bidlot, J., Bormann, N., Delsol, C., Dragani, R., Fuentes, M., Geer, A. J., Haimberger, L., Healy, S. B., Hersbach, H., Hólm, E. V., Isaksen, L., Kållberg, P., Köhler, M., Matricardi, M., McNally, A. P., Monge-Sanz, B. M., Morcrette, J.-J., Park, B.-K., Peubey, C., de Rosnay, P., Tavolato, C., Thépaut, J.-N., and Vitart, F.: The ERA-Interim reanalysis: configuration and performance of the data assimilation system, Q. J. Roy. Meteor. Soc., 137, 553–597, doi:10.1002/qj.828, 2011. 1403

Denton, G. H.: The Last Great Ice Sheets, John Wiley and Sons, New York, 1981. 1407, 1409

Dixon, E. J.: Human colonization of the Americas: timing, technology and process beringian Paleoenvironments – Festschrift in Honour of D. M. Hopkins, Quaternary Sci. Rev., 20, 277–299, doi:10.1016/S0277-3791(00)00116-5, 2001. 1397

Dupont, T. and Alley, R.: Assessment of the importance of ice-shelf buttressing to ice-sheet flow, Geophys. Res. Lett., 32, 1–4, doi:10.1029/2004GL022024, 2005. 1405, 1417

Fischer, H., Schmitt, J., Lüthi, D., Stocker, T. F., Tschumi, T., Parekh, P., Joos, F., Köhler, P., Völker, C., Gersonde, R., Barbante, C., Le Floch, M., Raynaud, D., and Wolff, E.: The role of Southern Ocean processes in orbital and millennial CO_2 variations – a synthesis, Quaternary Sci. Rev., 29, 193–205, 2010. 1397

Fisher, D. A. and Koerner, R. M.: On the special rheological properties of ancient microparticle-laden Northern Hemisphere ice as derived from bore-hole and core measurements, J. Glaciol., 32, 501–510, 1986. 1400

Forster, P.: Ice Ages and the mitochondrial DNA chronology of human dispersals: a review, Philos. T. R. Soc. B, 359, 255–264, 2004. 1397

Gallée, H., Van Yperselb, J., Fichefet, T., Marsiat, I., Tricot, C., and Berger, A.: Simulation of the last glacial cycle by a coupled, sectorially averaged climate-ice sheet model: 2. Response to insolation and CO_2 variations, J. Geophys. Res.-Atmos., 97, 15713–15740, 1992. 1398

Gent, P. R., Danabasoglu, G., Donner, L., Holland, M., Hunke, E., Jayne, S., Lawrence, D., Neale, R., Rasch, P., Vertenstein, M., Worley, P., Yang, Z.-L., and Zhang, M.: The Community Climate System Model version 4, J. Climate, 24, 4973–4991, 2011. 1401, 1402, 1416

ESDD
6, 1395–1443, 2015

An ice sheet model of reduced complexity for paleoclimate studies

B. Neff et al.

Gildor, H. and Tziperman, E.: A sea ice climate switch mechanism for the 100-kyr glacial cycles, J. Geophys. Res.-Oceans, 106, 9117–9133, 2001. 1397

Glen, J. W.: The creep of polycrystalline ice, P. Roy. Soc. Lond. A Mat., 228, 519–538, 1955. 1400

Greuell, W. and Konzelmann, T.: Numerical modelling of the energy balance and the englacial temperature of the Greenland Ice Sheet. Calculations for the ETH-Camp location (West Greenland, 1155 m a.s.l.), Global Planet. Change, 9, 91–114, doi:10.1016/0921-8181(94)90010-8, 1994. 1420

Greve, R.: A continuum–mechanical formulation for shallow polythermal ice sheets, Philos. T. R. Soc. A, 355, 921–974, doi:10.1098/rsta.1997.0050, 1997. 1404

Hays, J. D., Imbrie, J., and Shackleton, N. J.: Variations in the Earth's orbit: pacemaker of the ice ages, Science, 194, 1121–1132, 1976. 1418

Heinemann, M., Timmermann, A., Elison Timm, O., Saito, F., and Abe-Ouchi, A.: Deglacial ice sheet meltdown: orbital pacemaking and CO_2 effects, Clim. Past, 10, 1567–1579, doi:10.5194/cp-10-1567-2014, 2014. 1398, 1407, 1418

Herrington, A. R. and Poulsen, C. J.: Terminating the last interglacial: the role of ice sheet-climate feedbacks in a GCM asynchronously coupled to an Ice Sheet Model, J. Climate, 25, 1871–1882, 2011. 1398

Hofer, D., Raible, C., Merz, N., Dehnert, A., and Kuhlemann, J.: Simulated winter circulation types in the North Atlantic and European region for preindustrial and glacial conditions, Geophys. Res. Lett., 39, 1–5, doi:10.1029/2012GL052296, 2012. 1402, 1431

Hutter, K.: Theoretical glaciology: material science of ice and the mechanics of glaciers and ice sheets, vol. 1, Dordrecht a.o.: Reidel; Tokyo: Terra Scientific publishing Company, 1983. 1400

Huybers, P.: Early pleistocene glacial cycles and the integrated summer insolation forcing, Science, 313, 508–511, 2006. 1420

Huybers, P. and Wunsch, C.: Obliquity pacing of the late Pleistocene glacial terminations, Nature, 434, 491–494, 2005. 1418

Huybrechts, P.: Sea-level changes at the {LGM} from ice-dynamic reconstructions of the Greenland and Antarctic ice sheets during the glacial cycles, Quaternary Sci. Rev., 21, 203–231, doi:10.1016/S0277-3791(01)00082-8, 2002. 1401

Huybrechts, P. and de Wolde, J.: The dynamic response of the Greenland and Antarctic ice sheets to multiple-century climatic warming, J. Climate, 12, 2169–2188, 1999. 1402

ESDD
6, 1395–1443, 2015

An ice sheet model of reduced complexity for paleoclimate studies

B. Neff et al.

Huybrechts, P. and T'siobbel, S.: Thermomechanical modelling of Northern Hemisphere ice sheets with a two-level mass-balance parameterisation, Ann. Glaciol., 21, 111–116, 1995. 1402

Huybrechts, P., and Payne, T., and Intercomparison Group EISMINT: The EISMINT benchmarks for testing ice-sheet models, Ann. Glaciol., 23, 1–12, doi:10013/epic.12063, 1996. 1398, 1399, 1400, 1405, 1406, 1416, 1430, 1436

Imbrie, J. and Imbrie, J. Z.: Modeling the climatic response to orbital variations, Science, 207, 943–953, 1980. 1418

IPCC: Climate change 2007: the physical science basis, in: Contribution of Working Group I to the Fourth Assessment Report of the Intergovernmental Panel on Climate Change, edited by: Solomon, S., Qin, D., Manning, M., Chen, Z., Marquis, M., Averyt, K. B., Tignor M., and Miller, H. L., Cambridge University Press, Cambridge, UK and New York, NY, USA, 2007. 1405

Johnson, J. and Fastook, J. L.: Northern Hemisphere glaciation and its sensitivity to basal melt water, Quatern. Int., 95–96, 65–74, doi:10.1016/S1040-6182(02)00028-9, 2002. 1418

Kleman, J., Fastook, J., Ebert, K., Nilsson, J., and Caballero, R.: Pre-LGM Northern Hemisphere ice sheet topography, Clim. Past, 9, 2365–2378, doi:10.5194/cp-9-2365-2013, 2013. 1411, 1414

Li, C. and Battisti, D. S.: Reduced Atlantic storminess during last glacial maximum: evidence from a coupled climate model, J. Climate, 21, 3561–3579, doi:10.1175/2007JCLI2166.1, 2008. 1397

Lisiecki, L. E. and Raymo, M. E.: A Pliocene-Pleistocene stack of 57 globally distributed benthic δ18O records, Paleoceanography, 20, 2005. 1397

Loulergue, L., Schilt, A., Spahni, R., Masson-Delmotte, V., Blunier, T., Lemieux, B., Barnola, J.-M., Raynaud, D., Stocker, T. F., and Chappellaz, J.: Orbital and millennial-scale features of atmospheric CH_4 over the past 800,000 years, Nature, 453, 383–386, 2008. 1397

Lüthi, D., Le Floch, M., Bereiter, B., Blunier, T., Barnola, J.-M., Siegenthaler, U., Raynaud, D., Jouzel, J., Fischer, H., Kawamura, K., and Stocker, T. F.: High-resolution carbon dioxide concentration record 650,000–800,000 years before present, Nature, 453, 379–382, 2008. 1397

Masson-Delmotte, V., Schulz, M., Abe-Ouchi, A., Beer, J., Ganopolski, A., González Rouco, J. F., Jansen, E., Lambeck, K., Luterbacher, J., Naish, T., Osborn, T., Otto-Bliesner, B., Quinn, T., Ramesh, R., Rojas, M., Shao, X., and Timmermann, A.: Information from Paleoclimate

ESDD
6, 1395–1443, 2015
An ice sheet model of reduced complexity for paleoclimate studies
B. Neff et al.

Archives, in: Climate Change 2013: The Physical Science Basis, Contribution of Working Group I to the Fifth Assessment Report of the Intergovernmental Panel on Climate Change, edited by: Stocker, T. F., Qin, D., Plattner, G.-K., Tignor, M., Allen, S. K., Boschung, J., Nauels, A., Xia, Y., Bex, V., and Midgley, P. M., Cambridge University Press, Cambridge, UK and New York, NY, USA, 2013. 1420

Merz, N., Raible, C. C., Fischer, H., Varma, V., Prange, M., and Stocker, T. F.: Greenland accumulation and its connection to the large-scale atmospheric circulation in ERA-Interim and paleoclimate simulations, Clim. Past, 9, 2433–2450, doi:10.5194/cp-9-2433-2013, 2013. 1397, 1402, 1416, 1431

Merz, N., Born, A., Raible, C. C., Fischer, H., and Stocker, T. F.: Dependence of Eemian Greenland temperature reconstructions on the ice sheet topography, Clim. Past, 10, 1221–1238, doi:10.5194/cp-10-1221-2014, 2014a. 1397

Merz, N., Gfeller, G., Born, A., Raible, C. C., Stocker, T. F., and Fischer, H.: Influence of ice sheet topography on Greenland precipitation during the Eemian interglacial, J. Geophys. Res.-Atmos., 119, 10,749–10,768, doi:10.1002/2014JD021940, 2014b. 1397

Milankovitch, M.: Kanon der Erdbestrahlung und seine Anwendung auf das Eiszeitproblem, Belgrade, Royal Serbian Academy, 633 pp., 1941. 1397

Neale, R. B., Richter, J., Park, S., Lauritzen, P. H., Vavrus, S. J., Rasch, P. J., and Zhang, M.: The mean climate of the Community Atmosphere Model (CAM4) in forced SST and fully coupled experiments, J. Climate, 26, 5150–5168, doi:10.1175/JCLI-D-12-00236.1, 2013. 1402

Neeman, B. U., Ohring, G., and Joseph, J. H.: The Milankovitch theory and climate sensitivity: 2. Interaction between the Northern Hemisphere ice sheets and the climate system, J. Geophys. Res.-Atmos., 93, 11175–11191, 1988. 1398, 1416

Näslund, J., Rodhe, L., Fastook, J., and Holmlund, P.: New ways of studying ice sheet flow directions and glacial erosion by computer modelling examples from Fennoscandia, Quaternary Sci. Rev., 22, 245–258, doi:10.1016/S0277-3791(02)00079-3, 2003. 1398, 1416

Oerlemans, J.: Modeling of pleistocene European ice sheets: some experiments with simple mass-balance parameterizations, Quaternary Res., 15, 77–85, doi:10.1016/0033-5894(81)90115-0, 1981a. 1398, 1416

Oerlemans, J.: Some basic experiments with a vertically-integrated ice sheet model, Tellus, 33, 1–11, 1981b. 1397, 1398, 1399, 1401

Oerlemans, J.: Glacial cycles and ice-sheet modelling, Climatic Change, 4, 353–374, doi:10.1007/BF02423468, 1982. 1398

ESDD
6, 1395–1443, 2015

Paillard, D.: The timing of Pleistocene glaciations from a simple multiple-state climate model, Nature, 391, 378–381, doi:10.1038/34891, 1998. 1421

Pausata, F. S. R., Li, C., Wettstein, J. J., Kageyama, M., and Nisancioglu, K. H.: The key role of topography in altering North Atlantic atmospheric circulation during the last glacial period, Clim. Past, 7, 1089–1101, doi:10.5194/cp-7-1089-2011, 2011. 1397

Peltier, W. R.: On eustatic sea level history: Last Glacial Maximum to Holocene, Quaternary Sci. Rev., 21, 377–396, doi:10.1016/S0277-3791(01)00084-1, 2002. 1407, 1409

Peltier, W. R.: Global glacial isostasy and the surface of the ice-age Earth: the ICE-5G (VM2) model and GRACE, Annu. Rev. Earth Pl. Sc., 32, 111–149, doi:10.1146/annurev.earth.32.082503.144359, 2004. 1407, 1409, 1412, 1417, 1431, 1440

Plummer, M. A. and Phillips, F. M.: A 2-D numerical model of snow/ice energy balance and ice flow for paleoclimatic interpretation of glacial geomorphic features, Quaternary Sci. Rev., 22, 1389–1406, doi:10.1016/S0277-3791(03)00081-7, 2003. 1398

Pollard, D. and DeConto, R. M.: Hysteresis in Cenozoic Antarctic ice-sheet variations, Global Planet. Change, 45, 9–21, 2005. 1419

Quiquet, A., Ritz, C., Punge, H. J., and Salas y Mélia, D.: Greenland ice sheet contribution to sea level rise during the last interglacial period: a modelling study driven and constrained by ice core data, Clim. Past, 9, 353–366, doi:10.5194/cp-9-353-2013, 2013. 1420

Raymo, M. E. and Nisancioglu, K.: The 41 kyr world: Milankovitch's other unsolved mystery, Paleoceanography, 18, 1011, doi:10.1029/2002PA000791, 2003. 1397, 1420

Reeh, N.: Parameterization of melt rate and surface temperature on the Greenland Ice Sheet, Polarforschung, 59, 113–128, 1991. 1402, 1416

Reijmer, C. H. and Hock, R.: Internal accumulation on Storglaciären, Sweden, in a multi-layer snow model coupled to a distributed energy-and mass-balance model, J. Glaciol., 54, 61–72, 2008. 1420

Ritz, C., Fabre, A., and Letréguilly, A.: Sensitivity of a Greenland ice sheet model to ice flow and ablation parameters: consequences for the evolution through the last climatic cycle, Clim. Dynam., 13, 11–24, 1997. 1402

Ritz, S. P., Stocker, T. F., and Joos, F.: A coupled dynamical ocean–energy balance atmosphere model for paleoclimate studies, J. Climate, 24, 349–375, doi:10.1175/2010JCLI3351.1, 2011. 1420

ESDD
6, 1395–1443, 2015

Robinson, A., Calov, R., and Ganopolski, A.: Greenland ice sheet model parameters constrained using simulations of the Eemian Interglacial, Clim. Past, 7, 381–396, doi:10.5194/cp-7-381-2011, 2011. 1398, 1420

Schilt, A., Baumgartner, M., Blunier, T., Schwander, J., Spahni, R., Fischer, H., and Stocker, T. F.: Glacial-interglacial and millennial-scale variations in the atmospheric nitrous oxide concentration during the last 800,000 years, Quaternary Sci. Rev., 29, 182–192, doi:10.1016/j.quascirev.2009.03.011, 2010. 1397

Stocker, T. F.: The ocean as a component of the climate system, in: Ocean Circulation and Climate: A 21st Century Perspective, edited by: Siedler, G., Griffies, S. M., Gould, J., and Church, J. A., Academic Press, Amsterdam, 3–30, 2013. 1397

Siegert, M. J. and Marsiat, I.: Numerical reconstructions of LGM climate across the Eurasian Arctic, Quaternary Sci. Rev., 20, 1595–1605, 2001. 1398, 1416

Siegert, M. J., Dowdeswell, J. A., and Melles, M.: Late Weichselian Glaciation of the Russian High Arctic, Quaternary Res., 52, 273–285, doi:10.1006/qres.1999.2082, 1999. 1416, 1417

Smith, G., Mysak, L., Wang, Z., and Blatter, H.: McGill paleoclimate model ice sheet sensitivity to ice flow rate and discharge parameters, Clim. Dynam., 20, 315–325, doi:10.1007/s00382-002-0273-5, 2003. 1398

Spahni, R., Joos, F., Stocker, B. D., Steinacher, M., and Yu, Z. C.: Transient simulations of the carbon and nitrogen dynamics in northern peatlands: from the Last Glacial Maximum to the 21st century, Clim. Past, 9, 1287–1308, doi:10.5194/cp-9-1287-2013, 2013. 1397

Stokes, C. R., Tarasov, L., and Dyke, A. S.: Dynamics of the North American ice sheet complex during its inception and build-up to the Last Glacial Maximum, Quaternary Sci. Rev., 50, 86–104, doi:10.1016/j.quascirev.2012.07.009, 2012. 1411, 1414

Stone, E. J., Lunt, D. J., Annan, J. D., and Hargreaves, J. C.: Quantification of the Greenland ice sheet contribution to Last Interglacial sea level rise, Clim. Past, 9, 621–639, doi:10.5194/cp-9-621-2013, 2013. 1420

Svendsen, J. I., Alexanderson, H., Astakhov, V. I., Demidov, I., Dowdeswell, J. A., Funder, S., Gataullin, V., Henriksen, M., Hjort, C., Houmark-Nielsen, M., Hubberten, H. W., Ingólfsson, Ó., Jakobsson, M., Kjær, K. H., Larsen, E., Lokrantz, H., Lunkka, J. P., Lyså, A., Mangerud, J., Matiouchkov, A., Murray, A., Möller, P., Niessen, F., Nikolskaya, O., Polyak, L., Saarnisto, M., Siegert, C., Siegert, M. J., Spielhagen, R. F., and Stein, R.: Late Quaternary ice sheet history of northern Eurasia, Quaternary Sci. Rev., 23, 1229–1271, doi:10.1016/j.quascirev.2003.12.008, 2004. 1416, 1417

ESDD
6, 1395–1443, 2015

An ice sheet model of reduced complexity for paleoclimate studies

B. Neff et al.

Tarasov, L. and Peltier, W. R.: Impact of thermomechanical ice sheet coupling on a model of the 100 kyr ice age cycle, J. Geophys. Res.-Atmos., 104, 9517–9545, 1999. 1417

Verbitsky, M. Y. and Oglesby, R. J.: The effect of atmospheric carbon dioxide concentration on continental glaciation of the Northern Hemisphere, J. Geophys. Res.-Atmos., 97, 5895–5909, 1992. 1398

Waelbroeck, C., Labeyrie, L., Michel, E., Duplessy, J. C., McManus, J. F., Lambeck, K., Balbon, E., and Labracherie, M.: Sea-level and deep water temperature changes derived from benthic foraminifera isotopic records, Quaternary Sci. Rev., 21, 295–305, 2002. 1397

Xu-Ri and Prentice, I. C.: Terrestrial nitrogen cycle simulation with a dynamic global vegetation model, Glob. Change Biol., 14, 1745–1764, doi:10.1111/j.1365-2486.2008.01625.x, 2008. 1397

Ziemen, F. A., Rodehacke, C. B., and Mikolajewicz, U.: Coupled ice sheet–climate modeling under glacial and pre-industrial boundary conditions, Clim. Past, 10, 1817–1836, doi:10.5194/cp-10-1817-2014, 2014. 1410

ESDD

6, 1395–1443, 2015

An ice sheet model of reduced complexity for paleoclimate studies

B. Neff et al.

Table 1. Values of constants used in the ice model. The parameters that are used to tune the model are highlighted with a checkmark and therefore not constant between different members in the ensemble (Table 3). The values for the reference parameters set are given here.

Value	Quantity	Ensemble
$n = 3$	Flow-law exponent[a]	
$A = 10^{-16}\,\mathrm{Pa}^{-3}\,\mathrm{yr}^{-1}$	Flow-law parameter[a]	
$E = 1$	Flow enhancement parameter	✓
$T_{\mathrm{acc}} = 2\,^{\circ}\mathrm{C}$	Accumulation temperature	✓
$\beta = 6\,\mathrm{mm\,PDD}^{-1}$	Melting factor	✓
$g = 9.81\,\mathrm{m\,s}^{-2}$	Gravitational acceleration	
$\rho = 910\,\mathrm{kg\,m}^{-3}$	Ice density[a]	
$\tau_{\mathrm{br}} = 3000\,\mathrm{yr}$	Relaxation time for bedrock sinking	✓
$A_{\mathrm{ocean}} = 3.6 \times 10^{14}\,\mathrm{m}^2$	Ocean surface	
$\mathrm{SL}_{\mathrm{offset}} = 7.36\,\mathrm{m}$	Sea level offset for an ice free Greenland[b]	
$\Gamma = 6.5\,\mathrm{K\,km}^{-1}$	Temperature lapse rate	
$\lambda_{\mathrm{p}} = \ln(2)\,\mathrm{km}^{-1}$	Precipitation lapse rate[c]	

[a] Huybrechts et al. (1996), [b] Bamber et al. (2013), [c] Budd and Smith (1979)

ESDD
6, 1395–1443, 2015

Table 2. List of CCSM4 simulations of preindustrial (PI) and last glacial maximum (LGM) climates (Hofer et al., 2012; Merz et al., 2013) which are used as climate forcing in the ice model. Orbital parameters are calculated according to Berger (1978). Solar forcing is expressed as total solar irradiance (TSI). The LGM simulation uses the ICE-5G topography reconstruction (Peltier, 2004). All simulations have a time resolution of one day and a spatial resolution of one degree which is bi-linearly interpolated to the ice model resolution.

Simulation	Orbital parameters	SST/sea ice	CO_2 [ppm]	CH_4 [ppb]	N_2O [ppb]	TSI [$W m^{-2}$]	Ice sheets/topography
PD	present	PD	354	1694	310	1361.8	present
PI	present	PI	280	760	270	1360.9	present
LGM	21 ka	21 ka	185	350	200	1360.9	21 ka

ESDD
6, 1395–1443, 2015

An ice sheet model of reduced complexity for paleoclimate studies

B. Neff et al.

Table 3. Four tuning parameters with their used values. All possible combinations of parameter values result in 200 experiments which are run with two different versions of LGM climate forcing.

Name	Abbreviation	Unit	Values
Melting parameter	β	mm PDD^{-1}	5; 6; 7; 8; 9
Flow enhancement parameter	E	%	75; 100; 125; 150
Accumulation temperature	T_{acc}	°C	0; 1; 2; 3; 4
Bedrock relaxations time	τ_{br}	yr	3000; 6000

ESDD
6, 1395–1443, 2015

Table 4. Parameter distribution of the LGM_{bs} ensemble for all simulations consistent with LGM sea level reconstructions (see horizontal gray bar in Fig. 4, 114 members). Mean values: β = 5.97 mm PDD^{-1}, E = 111 %, T_{acc} = 2.09 °C, τ_{br} = 4526 yr.

Variable	Value	# Members									
β	5 mm PDD^{-1}	39	E	75 %	30	T_{acc}	0 °C	20	τ_{br}	3000 yr	56
	6 mm PDD^{-1}	40		100 %	30		1 °C	22		6000 yr	58
	7 mm PDD^{-1}	34		125 %	27		2 °C	24			
	8 mm PDD^{-1}	1		150 %	27		3 °C	24			
	9 mm PDD^{-1}	0					4 °C	24			

ESDD
6, 1395–1443, 2015
An ice sheet model of reduced complexity for paleoclimate studies
B. Neff et al.

Title Page
Abstract | Introduction
Conclusions | References
Tables | Figures
Back | Close
Full Screen / Esc
Printer-friendly Version
Interactive Discussion

Table 5. Subset of tuning parameters with 18 members and their used values for hysteresis ensemble (Fig. 8a).

Name	Abbreviation	Unit	Values
Melting parameter	β	mm PDD^{-1}	5; 6; 7
Accumulation temperature	T_{acc}	°C	2; 3; 4
Flow enhancement parameter	E	%	75; 100
Bedrock relaxation time	τ_{br}	yr	3000

ESDD
6, 1395–1443, 2015

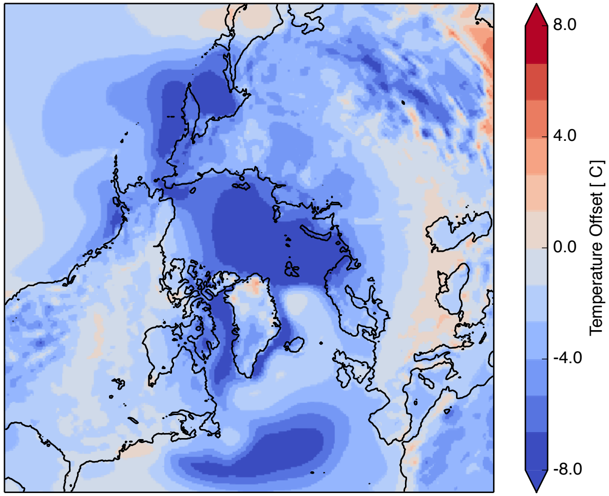

Figure 1. Difference between the CCSM4 PD and ERA-Interim temperature (CCSM4 PD – ERA-Interim), interpolated onto the ice sheet model grid. A general cold bias with an average of $-3.0\,^{\circ}$C is observed over the full domain. Largest offsets are found in regions with excessive sea ice in the model as well as in the path of the North Atlantic Current.

ESDD
6, 1395–1443, 2015

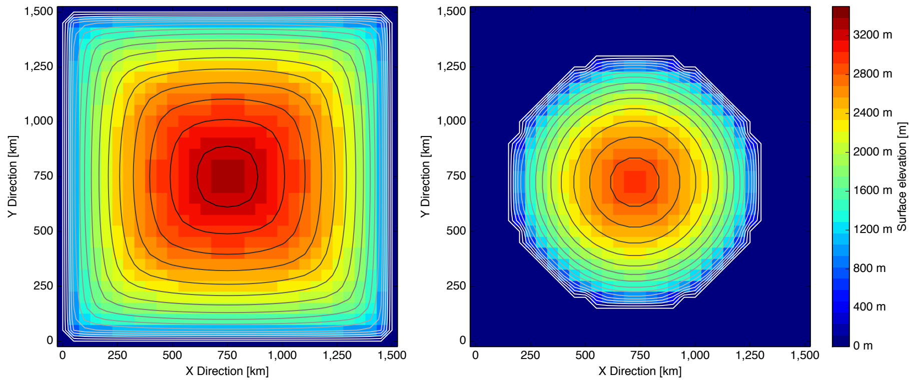

Figure 2. Results of the EISMINT$_{fixed}$ (left) and EISMINT$_{freemargin}$ (right) comparison at a steady state around 200 000 simulated years. Both images show ice surface elevation of the IceBern2D model with contour lines of 200 m equidistance. The EISMINT$_{fixed}$ is identical with the test from Huybrechts et al. (1996), the peak is in the center of the grid at an elevation of 3342.6 m. EISMINT$_{freemargin}$ has a deviation of 1 % from Huybrechts et al. (1996), the peak in the center is at 2925 m.

ESDD
6, 1395–1443, 2015

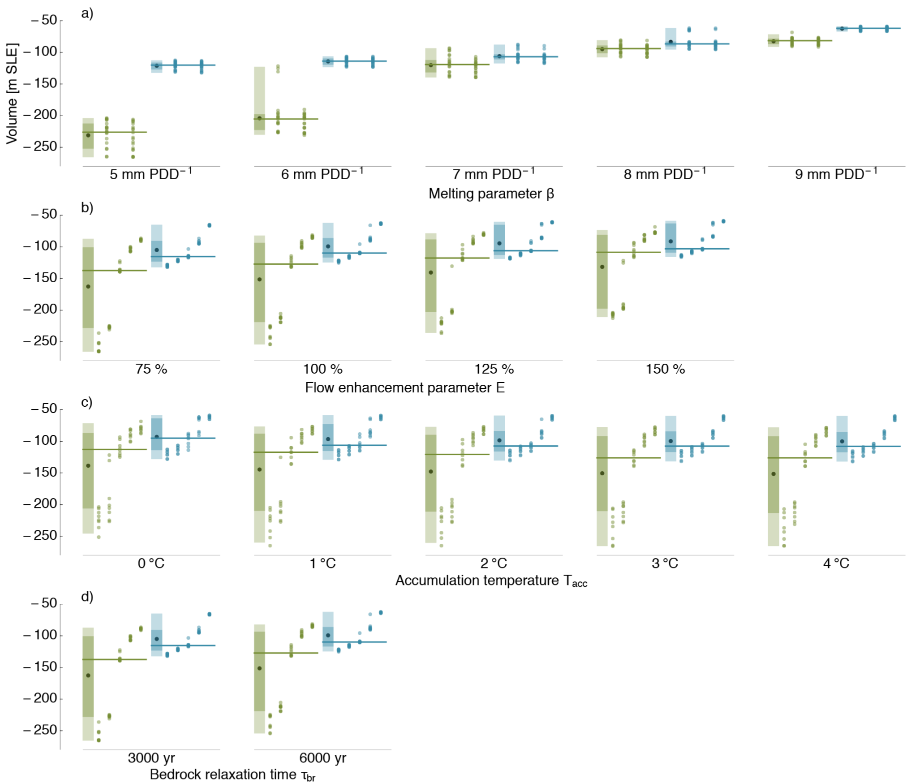

Figure 3. The dependence of the minimum sea level with respect to the different model parameters (rows) and climate forcing (green = LGM_{uc}, blue = LGM_{bs}). The light colored boxes contain 95 percent of the simulations, the darker box contains half of the total. The median is drawn as a line, the average as a black dot. The different columns of dots in one ensemble for panels **(b–d)** represent the 5 values of β, in panel **(a)**, ensembles for the two values of τ_{br} are shown.

ESDD
6, 1395–1443, 2015

An ice sheet model of reduced complexity for paleoclimate studies

B. Neff et al.

Title Page
Abstract | Introduction
Conclusions | References
Tables | Figures
◀I | ▶I
◀ | ▶
Back | Close
Full Screen / Esc
Printer-friendly Version
Interactive Discussion

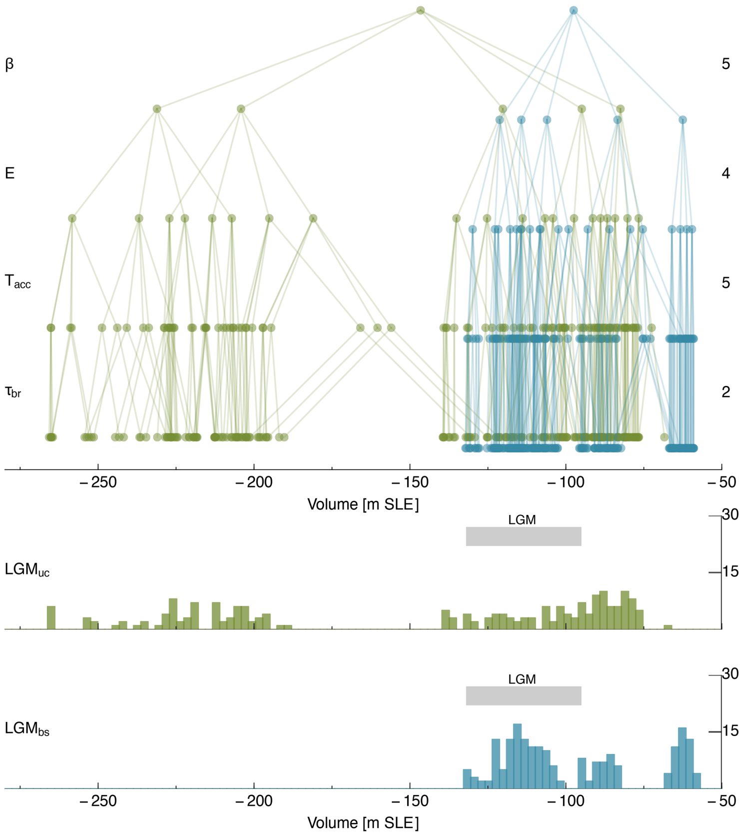

Figure 4. Structured parameter tree for the distribution of the minimum sea level with respect to the influence of each tuning parameter. Each layer is represented by a tuning parameter, the number of different tuning parameter values is shown on the right y axis. The gray horizontal bar corresponds to the sea level increase in the LGM on the Northern Hemisphere from Clark and Mix (2002).

ESDD
6, 1395–1443, 2015

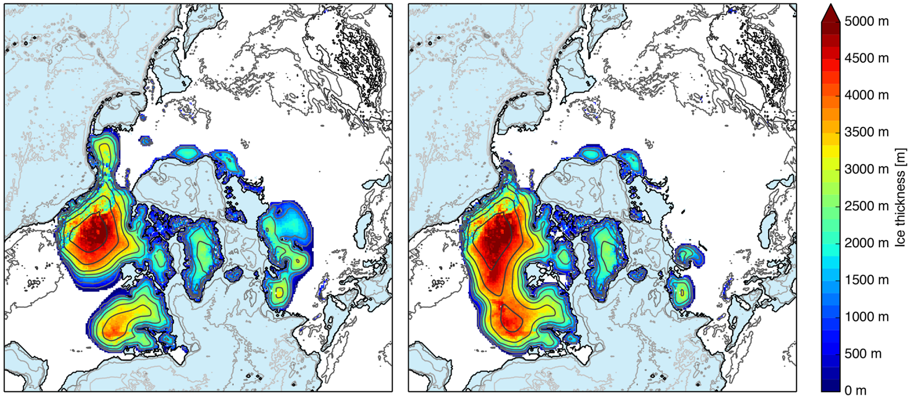

Figure 5. Ensemble composite of all simulations within LGM ice volume range of −132 and −95 m SLE (see gray horizontal bar in Fig. 4) (Clark and Mix, 2002). Ensemble LGM_{uc} (left, mean −111.9 m SLE) consists of 50 simulations, and LGM_{bs} climate forcing (right, mean −114.7 m SLE) has 114 members.

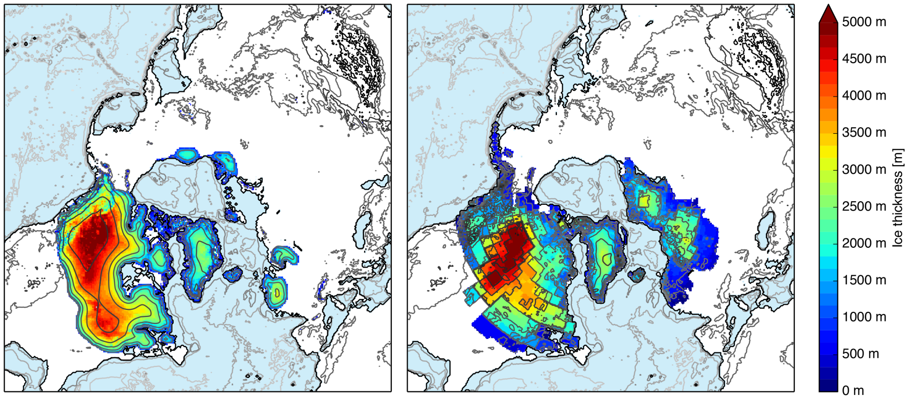

Figure 6. Simulation with the best-guess tuning parameters proximate to the mean values from Table 4 of all considered LGM_{bs} simulations within the LGM ice volume range (gray horizontal bar in Fig. 4) on the left. Parameters: $\beta = 6\,\mathrm{mm\,PDD^{-1}}$, $E = 100\,\%$, $T_{acc} = 2\,^{\circ}\mathrm{C}$, $\tau_{br} = 3000\,\mathrm{yr}$. Ice Volume: $-115\,\mathrm{m\,SLE}$. ICE-5G from Peltier (2004) with an ice volume of $117\,\mathrm{m\,SLE}$ on the Northern Hemisphere on the right.

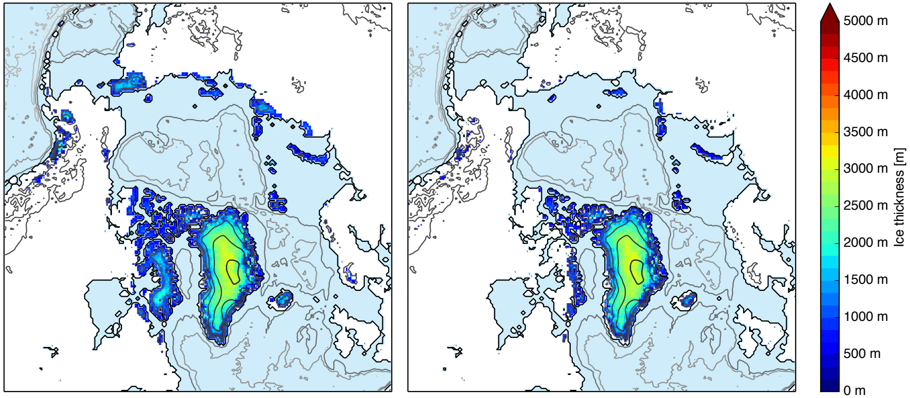

Figure 7. Ice distribution in the Northern Hemisphere for uncorrected preindustrial conditions (PI_{uc}, left) and with subtracted temperature bias (PI_{bs}, right). Simulated ice volumes correspond to −8.2 m SLE −4.1 m SLE, respectively, where the difference is mainly due to ice masses outside Greenland.

ESDD
6, 1395–1443, 2015

An ice sheet model of reduced complexity for paleoclimate studies

B. Neff et al.

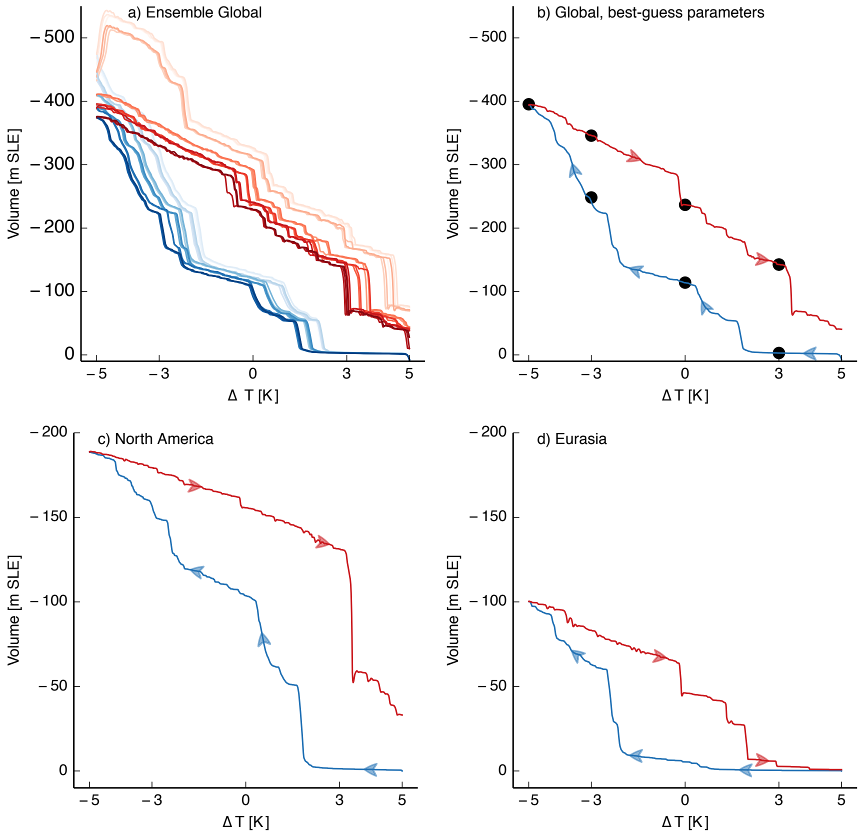

Figure 8. Global **(a, b)** and regional **(c, d)** ice volume as a function of global temperature offset. Increasing temperatures in blue, decreasing temperatures in red. On the top left **(a)** an ensemble with 18 Members (Table 5) indicating the robustness of the hysteresis behavior in a range of parameter values. All other plots **(b–d)** are from the simulation with the best-guess parameter (same as in Fig. 6, left). The dots denote **(b)** the ice volume in equilibrium at the specific temperature. Considered areas for Laurentide and Eurasia are highlighted in Fig. 9.

ESDD
6, 1395–1443, 2015

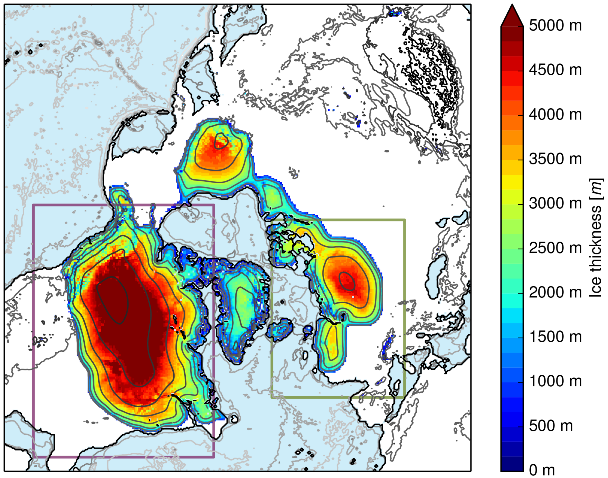

Figure 9. Hysteresis after 3.75 mio years at LGM temperature (Δ 0 °C) with an ice volume of 236.7 m SLE. The situation at the same temperature at the build up process of the ice sheet after 1.25 mio years can be seen in Fig. 6 (left). Areas of Laurentide and Eurasia from Fig. 8c and d are highlighted in purple and green.

ESDD
6, 1395–1443, 2015

An ice sheet model of reduced complexity for paleoclimate studies

B. Neff et al.